AUT Journal of Mathematics and Computing

AUT J. Math. Comput., 6(2) (2025) 97-108
https://doi.org/10.22060/AJMC.2024.22987.1212

Original Article

Non-oscillatory central schemes for the Saint-Venant system

Rooholah Abedian*[a]

[a]*School of Engineering Science, College of Engineering, University of Tehran, Iran*

ABSTRACT: The research aims to develop a well-balanced numerical method for solving the shallow water equations, which account for the balance laws and the source term related to the seabed slope. The proposed method combines a Runge-Kutta scheme for accurate time integration and the natural continuous extension method for spatial discretization. To achieve high-order spatial accuracy, the method employs central non-staggered (CNS) reconstructions of the conservative variables and the water surface elevation. This is achieved through two key steps. The initial step involves determining the specific values of the flux derivative and the bed slope source term at individual points. The subsequent step entails integrating the source term spatially. Both of these steps are designed to preserve the C-*property*, which ensures the exact preservation of the quiescent flow solution. The method is verified using a variety of standard one-dimensional test cases, including smooth and discontinuous solutions, to demonstrate its accuracy and resolution properties.

Review History:
Received:09 February 2024
Revised:10 August 2024
Accepted:14 August 2024
Available Online:01 March 2025

Keywords:
Central schemes
Shallow water equations
Source terms
C-property

MSC (2020):
35L65; 65D05; 76M20

1. Introduction

In recent times, the field of fluid mechanics and hydraulic engineering has seen the notable usage of advanced techniques with high-resolution capabilities to tackle the shallow water equations (SWE) [16, 21]. Specifically, the Godunov-type finite volume methods have made significant advancements, enabling their practical implementation in a variety of engineering scenarios.

In the field of numerical methods for solving SWE, there has been a particular focus on using coarse grids for numerical integration when studying hyperbolic systems of conservation laws from a fundamental research standpoint. This approach allows for an increasing level of accuracy in the computations. The development of high-order numerical techniques, specifically the essentially non-oscillatory (ENO) methods, has seen significant advancements in the field. These methods have evolved from the groundbreaking research conducted by Harten et al. [7] and have since progressed into weighted essentially non-oscillatory (WENO) schemes. The foundational contributions by authors of [10, 14] have played a crucial role in shaping this field. Numerous fifth-order WENO schemes have been presented as methods for addressing the challenges of solving conservation laws. These schemes have been proposed by various researchers, including [1, 2, 3, 19, 20, 27, 28]. Furthermore, Yamaleev and Carpenter have made significant contributions in this field by developing a sixth-order WENO scheme [25].

*Corresponding author.
E-mail addresses: rabedian@ut.ac.ir

The central schemes have gained increasing popularity in recent years due to their simplicity. These techniques function without requiring explicit understanding of the eigenstructure of a particular problem and do not rely on the utilization of Riemann solvers. In 1990, Nessyahu and Tadmor [17] introduced a central method called the NT scheme, which is a second-order method. This approach enhances the first-order Lax-Friedrichs method by utilizing the construction of piecewise-linear MUSCL-type interpolants from piecewise constant data. To prevent oscillations, non-linear limiters are utilized. Kurganov and Tadmor [11] later proposed modifications to the NT scheme, aiming to reduce the amount of numerical viscosity. Building on this, in 1996, the authors of [13] developed a technique called the non-oscillatory third-order reconstruction, which served as the foundation for the introduction of third-order central schemes. Liu and Tadmor [15] then put forth a staggered evolution approach for the reconstructed cell averages within these schemes, demonstrating that this third-order extension maintains non-oscillatory behavior by not increasing the number of initial extrema. More recently, Peer et al. [18] presented a fourth-order central method designed specifically for solving hyperbolic systems of conservation laws. They extended the NT method and developed a novel approach that combines a higher-order polynomial with a mechanism to effectively remove undesirable oscillations in the solution.

In recent years, the simplicity of central schemes has led to their increasing popularity. These techniques function without requiring explicit understanding of the eigen-structure of a particular problem and do not rely on the utilization of Riemann solvers. In 1990, Nessyahu and Tadmor [17] introduced a central method called the NT scheme, which is a second-order method. This approach enhances the first-order Lax-Friedrichs method by utilizing the construction of piecewise-linear MUSCL-type interpolants from piecewise constant data. To prevent oscillations, non-linear limiters are utilized. Kurganov and Tadmor [11] proposed modifications to the NT scheme, aiming to reduce the amount of numerical viscosity. In 1996, authors of [13] developed a technique called the non-oscillatory third-order reconstruction which served as the foundation for the introduction of third-order central schemes. Building upon this, Liu and Tadmor [15] put forth a staggered evolution approach for the reconstructed cell averages within these schemes. They demonstrated that this third-order extension maintains non-oscillatory behaviour by not increasing the number of initial extrema. In their work, Peer et al. [18] presented a fourth-order central method designed specifically for solving hyperbolic systems of conservation laws. They extended the NT method and developed a novel approach that combines a higher-order polynomial with a mechanism to effectively remove undesirable oscillations in the solution.

In recent years, there has been significant research focused on effectively handling the source term arising from the bed slope in shallow flow equations. The presence of this source term often leads to instability, particularly when the bottom elevation in real topography is uneven. Vuković and Sopta [23] published a paper that addressed the shallow water equations. To achieve momentum flux balance with the source term, they utilized an ENO-WENO approach. This approach was based on a method initially proposed in [4] and further improved by Vázquez-Cendón [22]. The effects of source terms resulting from cross-section irregularities were investigated in [6]. Additionally, Hubbard and Garcia-Navarro conducted an analysis on the effects of additional terms (or external factors) within a flux difference splitting approach. The authors of [23] were able to precisely satisfy the C-*property* [4, 22], although the method was complex. An alternative approach was utilized by LeVeque [12] in the nearly constant wave propagation scheme, incorporating a Riemann problem at the centre of each cell to achieve balance.

This paper introduces a fourth-order central non-staggered method designed for simulating the one-dimensional shallow water system of balance laws with a bed slope source term. The key advantage of the proposed approach is its broad applicability across various engineering scenarios. Specifically, this method can be employed in civil engineering problems using one-dimensional (1D) and two-dimensional (2D) computational models that utilize the shallow water equations (SWE), as referenced in [21] and other cited sources. The central non-staggered method presented in this paper provides a high-order numerical scheme for accurately simulating the shallow water system, including the handling of the bed slope source term. This makes the method suitable for a wide range of civil engineering applications that involve the use of the shallow water equations, such as river and flood modeling, coastal engineering, and hydraulic infrastructure design.

The structure of this document is as follows: In the next section (Section 2), a detailed explanation of the fourth-order central non-staggered method will be provided for the 1D shallow water equations. Section 3 will present several numerical examples to evaluate the performance of this approach. The final section (Section 4) will contain the concluding remarks.

2. CNS4 for Shallow water equation

Under the assumption of classical hypothesis, the one-dimensional SWE can be represented by

$$u_t + f(u)_x = s, \tag{1}$$

where $u = (h, vh)^T$, $f(u) = (vh, gh^2/2 + v^2h)^T$ and $s = (0, ghs_0)^T$. Here, the function $h(x,t)$ represents the depth of the flowing substance, while $v(x,t)$ represents the average velocity in the vertical direction. The symbol g is the gravity, $s_0 = -dz/dx$ is the bottom slope and $z(x)$ is the bottom elevation. In the upcoming discussion, each vector operation must be intended *component-wise*. To discretize the computational domain in space, a spatial step size of Δx is used. The domain is divided into a grid of uniformly spaced points, where each point is defined as $x_j = j\Delta x$. Additionally, a staggered grid is introduced, where the points are defined as $x_{j+1/2} = (j + 1/2)\Delta x$. To ensure numerical stability, each computational step has a time interval of Δt, where t^n represents the time at which the known variables are evaluated. By adding the time step size Δt to the current time t^n, we obtain the evaluation time t^{n+1} for the unknown variables. The jth cell, denoted as $I_j = [x_{j-1/2}, x_{j+1/2}]$, corresponds to a region focused on the grid point x_j. In this context, $\bar{u}_j^n$ refers to the average value of the solution within the cell at time t^n, while $\bar{s}_j$ represents the average value of the source term within the cell. Integrating (1) over $I_{j+1/2} \times [t^n, t^{n+1}]$ yields:

$$\bar{u}_{j+1/2}^{n+1} = \bar{u}_{j+1/2}^{n} - \frac{1}{\Delta x}\int_{t^n}^{t^{n+1}} \Big(f(u(x_{j+1},t)) - f(u(x_j,t))\Big)dt + \int_{t^n}^{t^{n+1}} \bar{s}_{j+1/2}dt. \tag{2}$$

Remark 2.1. *Eq. (2) characterizes the progression from t^n to t^{n+1} within staggered methods. The existing state of the system, which is represented by the average solution within each cell on the original grid, undergoes modifications on the shifted grid. An additional procedure is incorporated, where the revised solution $\bar{u}_{j+1/2}^{n+1}$ is mapped back onto the original grid in order to derive $\bar{u}_j^{n+1}$. This step helps ensure consistency with the grid structure and allows for the solution to be represented at the original grid points (this is the non-staggered version of central schemes, for more information, refer to [9]).*

To attain a level of accuracy in time known as fourth-order, a decision is made to employ the Simpson's quadrature rule. By adopting this approach, the time integrals of Eq. (2) can be expressed as follows:

$$\bar{u}_{j+1/2}^{n+1} = \bar{u}_{j+1/2}^{n} - \frac{\Delta t}{\Delta x}\sum_{l=1}^{3} N_l\Big(f(\hat{u}(x_{j+1}, t^{n+\beta_l})) - f(\hat{u}(x_j, t^{n+\beta_l})) - \Delta x \bar{s}_{j+1/2}^{n+\beta_l}\Big), \tag{3}$$

where

$$\bar{s}_{j+1/2}^{n+\beta_l} = \frac{1}{\Delta x}\int_{x_j}^{x_{j+1}} s(x, t^n + \beta_l \Delta t)dx. \tag{4}$$

Moreover, the weights employed in the quadrature can be denoted as $(N_1, N_2, N_3) = (\frac{1}{6}, \frac{4}{6}, \frac{1}{6})$, while the nodes associated with the quadrature are represented as $(\beta_1, \beta_2, \beta_3) = (0, \frac{1}{2}, 1)$. In addition, the estimated point-value solution, denoted as $\hat{u}$, is derived using a fourth-order Runge-Kutta scheme. The $\hat{u}^{n+1}$, as stated in Eq. (3), can be written as follows:

$$\hat{u}^{n+1} = \hat{u}^n + \Delta t\sum_{i=1}^{4} b_i k^{(i)}, \qquad \hat{u}^{(i)} = \hat{u}^n + \Delta t\sum_{j=1}^{i} a_{ij}k^{(j)}, \tag{5}$$

where

$$\mathbf{b} = \begin{pmatrix} 1/6 \\ 1/3 \\ 1/3 \\ 1/6 \end{pmatrix}, \qquad \mathbf{a} = \begin{pmatrix} 0 & 0 & 0 & 0 \\ 1/2 & 0 & 0 & 0 \\ 0 & 1/2 & 0 & 0 \\ 0 & 0 & 1 & 0 \end{pmatrix},$$

and $k^{(i)}$ are the Runge-Kutta fluxes. In the context of the balance law (1), the numerical evaluation of $(-f_x + s)$ is denoted as $k^{(i)}$. This evaluation is computed based on the point-values $\hat{u}^{(i)}$. Furthermore, $\hat{u}^{n+1/2}$ in Eq. (3) is determined employing the NCE (natural continuous extension) within the RK method [26]. The expression is given by:

$$\hat{u}^{n+1/2} = \hat{u}^n + \Delta t(5/24k^{(1)} + 1/6k^{(2)} + 1/6k^{(3)} - 1/24k^{(4)}).$$

2.1. Fourth-order non-oscillatory reconstruction

The method proposed by Zhou et al. [29], known as the surface gradient method (SGM), is employed in this study. By choosing $\eta = h + z$ as the benchmark level for the free surface, precise values of the conservative variables at the center of the cells are guaranteed. This choice effectively balances the flux gradient and the source term associated with the bottom slope. It helps maintain the accuracy of the solution and ensures proper handling of the dynamics between the variables involved. The vector of reconstructed variables $\mu = (\eta, vh)^T$ is introduced. The overall process can be briefly outlined as follow:

(I) The computed quantities of $\bar{\mu}_j$ are obtained by adding $\bar{z}_j$ to the first component of $\bar{u}_j$.

(II) Appropriate polynomials $P_j(x)$ are established, and the intended reconstruction takes the form of a piecewise function across the mesh I_j:

$$w(x,t^n)=\sum_j P_j(x)\chi_j(x), \qquad \chi_j(x):=1_{I_j}. \tag{6}$$

After obtaining $w(x,t^n)$, $\bar{\mu}_{j+1/2}$ is computed using:

$$\bar{\mu}_{j+1/2}=\int_{I_{j+1/2}} w(\zeta,t^n)d\zeta=\int_{x_j}^{x_{j+1/2}} w(\zeta,t^n)d\zeta+\int_{x_{j+1/2}}^{x_{j+1}} w(\zeta,t^n)d\zeta,$$

and $\hat{\mu}_j$ is computed using:

$$\hat{\mu}_j=w(x_j,t^n)=P_j(x_j).$$

(III) The computation of the cell-averaged values $\bar{u}^n_{j+1/2}$ involves subtracting $\bar{z}_{j+1/2}$ from the first component of $\bar{\mu}^n_{j+1/2}$. The computation of the point-values of $\hat{u}^n_j$ involves subtracting z_j from the first component of $\hat{\mu}^n_j$.

Peer et. al considered the cubic polynomial $P_j(x)$ on I_j for the fourth-order reconstruction as follows [18]:

$$P_j(x)=\mu^n_j+\mu'_j(\frac{x-x_j}{\Delta x})+\frac{1}{2!}\mu''_j(\frac{x-x_j}{\Delta x})^2+\frac{1}{3!}\mu'''_j(\frac{x-x_j}{\Delta x})^3,$$

where $\mu^n_j, \mu'_j/\Delta x, \mu''_j/(\Delta x)^2$, and $\mu'''_j/(\Delta x)^3$ denote the approximated values as well as the first, second, and third derivatives of $\mu(x,t^n)$ at $x=x_j$. These approximations are obtained by reconstructing the values using the cell averages $\{\bar{\mu}^n_j\}$. There are different methods for approximating these numerical derivatives. It is crucial to emphasize that the reconstruction process needs to satisfy:

1. $\mathcal{P}1-$ Conservation of cell averages: $\frac{1}{\Delta x}\int_{x_{j-1/2}}^{x_{j+1/2}} P_j(x)dx=\bar{\mu}^n_j$,
2. $\mathcal{P}2-$ Accuracy: $\mu(x,t^n)=u(x,t^n)+\mathcal{O}(\Delta x^4)$,
3. $\mathcal{P}3-$ Non-oscillatory behaviour: $w(x,t^n)=\sum_j P_j(x)\chi_j(x)$ should exhibit non-oscillatory behaviour.

Remark 2.2. *By ensuring the conservation of cell averages, maintaining high-order accuracy, and enforcing non-oscillatory behavior in the reconstruction process, the central scheme can effectively capture the complex wave dynamics and propagation of solutions for hyperbolic conservation law problems, such as the shallow water equations. These properties are essential for the numerical scheme to provide reliable and accurate results, which are crucial for various applications, such as fluid dynamics, atmospheric modeling, and coastal engineering.*

To ensure the fulfilment of property $\mathcal{P}1$, the reconstructed values μ^n_j need to satisfy the following condition:

$$\mu^n_j=\bar{\mu}^n_j-\frac{\mu''_j}{24}. \tag{7}$$

The NT scheme (Nessyahu-Tadmor scheme) [17] employs a limiter that achieves second-order accuracy for the numerical derivative μ'_j. The specific form of this limiter is as follows:

$$\mu'_j=\mathbf{MM}(\Delta\bar{\mu}_{j-1/2},\Delta\bar{\mu}_{j+1/2}), \tag{8}$$

where $\Delta\bar{\mu}_{j+1/2}=\bar{\mu}_{j+1}-\bar{\mu}_j$. The MinMod limiter, denoted as $\mathbf{MM}$, is defined as follows:

$$\mathbf{MM}(x_1,x_2,\dots)=\begin{cases}\min\{x_n\}, & x_n>0,\\ \max\{x_n\}, & x_n<0,\\ 0, & \text{otherwise.}\end{cases}$$

Please note that the accuracy of (8) decreases when $\Delta\bar{\mu}_{j-1/2}.\Delta\bar{\mu}_{j+1/2}<0\neq\mu'_j$. The NT method enhances the UNO (uniform non-oscillatory) limiter proposed in [8] by incorporating second-order differences into (8) in order to achieve higher accuracy:

$$\mu'_j=\mathbf{MM}\Big(\Delta\bar{\mu}_{j-1/2}+\frac{1}{2}\mathbf{MM}(\Delta^2\bar{\mu}_{j-1},\Delta^2\bar{\mu}_j),\Delta\bar{\mu}_{j+1/2}-\frac{1}{2}\mathbf{MM}(\Delta^2\bar{\mu}_j,\Delta^2\bar{\mu}_{j+1})\Big),$$

where $\Delta^2\bar{\mu}_j=\Delta\bar{\mu}_{j+1/2}-\Delta\bar{\mu}_{j-1/2}$.

The authors in [18] employ the modified UNO limiter to fulfill properties $\mathcal{P}2-\mathcal{P}3$. Just like the numerical derivative (8), μ'''_j is influenced by the adjacent third-order differences

$$\mu'''_j=\mathbf{MM}(\Delta^3\bar{\mu}^n_{j-1/2},\Delta^3\bar{\mu}^n_{j+1/2}),$$

where $\Delta^3\bar{\mu}^n_{j+1/2} = \Delta^2\bar{\mu}^n_{j+1} - \Delta^2\bar{\mu}^n_j$. Just like the UNO limiter, they implemented a method to acquire first derivative approximations with fourth-order accuracy, and this involved

$$\mu'_j = \mathbf{MM}\Big(\Delta\bar{\mu}^n_{j-1/2} + \frac{1}{2}\mathbf{MM}(\Delta^2\bar{\mu}^n_{j-1} + \frac{7}{12}\mu'''_{j-1}, \Delta^2\bar{\mu}^n_j - \frac{5}{12}\mu'''_j), \\ \Delta\bar{\mu}^n_{j+1/2} - \frac{1}{2}\mathbf{MM}(\Delta^2\bar{\mu}^n_j + \frac{5}{12}\mu'''_j, \Delta^2\bar{\mu}^n_{j+1} - \frac{7}{12}\mu'''_{j+1})\Big).$$

To estimate the values μ^n_j at individual points in (7) based on the average values within each cell, Peer et al. put

$$\mu''_j = \mathbf{MM}(\Delta^2\bar{\mu}^n_{j-1} + \mu'''_{j-1}, \Delta^2\bar{\mu}^n_j, \Delta^2\bar{\mu}^n_{j+1} - \mu'''_{j+1}).$$

2.2. Reconstruction of $k^{(i)}$

Here, the evaluation of Runge-Kutta fluxes, necessary in Eq. (5), is performed. This method enables the C-*property* achievement. The fundamental component involves introducing a suitable cell function $K_j(x, u(x,t))$ considered by

$$K_j(x, u(x,t)) = -\begin{pmatrix} (vh) - (vh)_j \\ (v^2h + 1/2g(\eta - z)^2) - (v^2h + 1/2g(\eta - z)^2)_j \end{pmatrix} + \begin{pmatrix} 0 \\ 1/2((\eta_j - z)^2 - (\eta_j - z_j)^2) \end{pmatrix}.$$

The $K_j(x, u(x,t))$ is considered in such a way that it fulfils the following two analytical relationships:

$$\frac{\partial K_j}{\partial x}\bigg|_{x=x_j} = k_j = (-f_x + s)_j,$$

and, in situations where there is no fluid movement (i.e., when $vh = 0$ and η remains unchanged):

$$K_j(x) = 0 \qquad \forall x.$$

By considering $T(x, t^n)$ as the reconstruction of $K_j(x, u(x,t))$, which is determined by an equation that is formally equivalent to (6), the approximation of the Runge-Kutta fluxes at x_j must be given by $T'(x_j, t^n)$(i.e. $k_j \approx T'(x_j, t^n)$).

2.3. Approximation of $\bar{s}^{n+\beta_l}_{j+1/2}$

In Eq. (4), the integration is required to be applied at three different time points: $t^{n+\beta_l}$ with $(\beta_0, \beta_1, \beta_2) = (0, 1/2, 1)$. The initial step entails performing analytical manipulations on the second component of the integration of the bed slope source term, as described in [5]:

$$\Delta x\bar{s}^{[2]}_{j+1/2} = -\int_{x_j}^{x_{j+1}} gh\frac{dz}{dx}dx, \tag{9}$$

applying the relationship $h = \eta - z$ and applying the straightforward integration by parts technique:

$$\Delta x\bar{s}^{[2]}_{j+1/2} = -\int_{x_j}^{x_{j+1}} gh\frac{dz}{dx}dx = -\int_{x_j}^{x_{j+1}} g(\eta - z)\frac{dz}{dx}dx \\ = \frac{1}{2}g\Big[z^2_{j+1} - z^2_j\Big] - g\Big[\eta_{j+1}z_{j+1} - \eta_j z_j\Big] + \int_{x_j}^{x_{j+1}} gz\frac{d\eta}{dx}dx,$$

and demonstrating $\xi(x) = gz\frac{d\eta}{dx}$:

$$\Delta x\bar{s}^{[2]}_{j+1/2} = \frac{1}{2}g\Big[z^2_{j+1} - z^2_j\Big] - g\Big[\eta_{j+1}z_{j+1} - \eta_j z_j\Big] + \int_{x_j}^{x_{j+1}} \xi(x)dx. \tag{10}$$

Eqs. (9) and (10) exhibit analytical equivalence; however, they manifest numerical dissimilarity. The Eq. (9) requires integration with respect to bed spatial derivatives, while the Eq. (10) requires integration with respect to free-surface spatial derivatives. When addressing a bed configuration that is non-uniform or uneven, the formulation (10) is preferred because the spatial derivative of the free-surface elevation is smoother compared to that of the bed elevation. This smoother nature of the derivative contributes to the formulation's favorability, despite the possibility of the solution itself being discontinuous. Consequently, this leads to a reduction in the overall error in the numerical computation. When dealing with a regular bottom, both methods produce comparable outcomes, allowing us to

employ the Eq. (10) formulation once again. In this study, we carry out the integration of the source term by (10). The computation of the first two terms on the RHS of (10) presents no challenges for the time instances $t^{n+\beta_l}$ with $(\beta_0, \beta_1, \beta_2) = (0, 1/2, 1)$, as the accurate computation of these values can be achieved by utilizing the point values z_j and $\hat{\eta}_j$. Only the final term requires a particular numerical approach. This integration procedure comprises three steps: first, the derivatives of the point values $\hat{\eta}'_j$ are reconstructed based on $\hat{\eta}_j$; next, the point $\hat{\xi}_j = (gz\frac{d\eta}{dx})_j$ are obtained using this foundation; finally, the integral is approximated employing a non-oscillatory reconstruction. All of these steps satisfy the non-oscillatory requirements, as elaborated in the subsequent explanation:

(1) the integration of the source term at times $t^{n+\beta_l}$ requires reconstructing the derivatives of the free-surface point-values $\hat{\eta}'_j$ from $\hat{\eta}_j$. To accomplish this, a non-oscillatory reconstruction technique, similar to the one described in subsection 2.2, is employed, where $\eta(x)$ is replaced with $K_j(x, u(x,t))$. Finally, evaluating of $\xi(x)$ at each time level can be expressed as:

$$\hat{\xi}_j = (gz\frac{d\eta}{dx})_j = gz_j\hat{\eta}'_j.$$

(2) the calculation of the integral in (10) relies on a non-oscillatory reconstruction of $\xi(x)$, which is fully compatible with the remaining reconstructions. Introducing,

$$M_{j+1/2}(x) = m^n_{j+1/2} + m'_{j+1/2}(\frac{x - x_{j+1/2}}{\Delta x}) + \frac{1}{2!}m''_{j+1/2}(\frac{x - x_{j+1/2}}{\Delta x})^2 + \frac{1}{3!}m'''_{j+1/2}(\frac{x - x_{j+1/2}}{\Delta x})^3,$$

The expression for reconstructing $\xi(x)$ on $I_{j+1/2}$ is as follows:

$$L(x, t^n) = \sum_j M_{j+1/2}(x)\chi_{j+1/2}.$$

The $\bar{\xi}_{j+1/2}$ on $I_{j+1/2}$ can be calculated as follows:

$$\bar{\xi}_{j+1/2} = \frac{1}{\Delta x}\int_{x_j}^{x_{j+1}} L(x, t^n)dx = \frac{1}{\Delta x}\int_{x_j}^{x_{j+1}} M_{j+1/2}(x)dx.$$

Once $\bar{\xi}_{j+1/2}$ is calculated, the $\bar{s}_{j+1/2}$ can be evaluated employing as follows:

$$\bar{s}_{j+1/2} = \begin{pmatrix} 0 \\ \frac{g}{2\Delta x}(z^2_{j+1} - z^2_j) - \frac{g}{\Delta x}(\hat{\eta}_{j+1}z_{j+1} - \hat{\eta}_j z_j) + \bar{\xi}_{j+1/2} \end{pmatrix}.$$

Remark 2.3. *The scheme suggested in this study can fulfill the C-property, specifically the equation $\bar{u}^{n+1}_j = \bar{u}^n_j$, given that $\eta = \eta^* =$ constant and $vh = 0$. For further information and a demonstration of this property, see [5].*

3. Computational results

This section presents the numerical outcomes obtained using the central non-staggered scheme (CNS4). The chosen test cases facilitate a thorough examination of various aspects of the method. An adaptive time step to ensure the numerical stability is employed, which satisfies the CFL-like condition represented by the equation:

$$\Delta t = C\frac{\Delta x}{\max_j\left(|\hat{v}^n_j| + \sqrt{g\hat{h}^n_j}\right)}.$$

In this context, $\hat{h}^n_j$ and $\hat{v}^n_j$ represent the reconstructed point values of flow depth and flow velocity at time t^n. The constant $C = 0.4$ is utilized.

Example 3.1. *The test case used to validate the fourth-order spatial accuracy of the scheme involves simulating steady sub-critical flow over a Gaussian bump in a channel that is* 30 *meters long. The elevation of the channel bed is described by the Gaussian function $z(x)$, given by*

$$z(x) = \frac{c_0}{\sigma\sqrt{2\pi}}\exp\left(-\frac{1}{2}(\frac{x - x_m}{\sigma})\right)^2,$$

where $c_0 = 1m^2$, $\sigma = 2m$, and $x_m = 15m$. The initial conditions include a constant water level of 2 *meters and zero discharge. The prescribed boundary conditions at the upstream and downstream are defined as $q = 4.42m^2/s$ and $h = 2m$, respectively. This test case, designed specifically for accuracy analysis, ensures that there are no discontinuities in the bed elevation or hydraulic variables. Table 1 presents the results of the accuracy analysis for the free-surface elevation η. The analysis confirms that the scheme achieves fourth-order accuracy according to each norm, thereby validating the expected spatial accuracy of the scheme. Comparable outcomes, which are not presented here, are achieved when examining the specific discharge.*

Table 1: Errors and orders of convergence for Example 3.1 (the free-surface elevation)

N	L_1 error	L_1 order	L_∞ error	L_∞ order
40	5.43(-4)	—	1.18(-3)	—
80	2.71(-5)	4.32	1.21(-4)	3.28
160	1.32(-6)	4.36	9.73(-6)	3.64
320	9.20(-8)	3.84	6.07(-7)	4.00
640	6.42(-9)	3.84	5.14(-8)	3.56

Example 3.2. *The scheme's fourth-order accuracy in both space and time, obtained in smooth areas of the solution, is validated applying Xing and Shu's proposed test case [24]. The shape of the seafloor is represented by the function* $z(x) = \sin^2(\pi x)$*, while the initial functions are provided by the following equations:*

$$h(x,0) = 5 + \exp(\cos(2\pi x)); \qquad vh(x,0) = \sin(\cos(2\pi x)), \qquad x \in [0,1]m.$$

In this situation, we assume periodic boundary conditions. As the test lacks an analytical solution, the "reference solution" used is a numerical solution obtained from a fine mesh comprising $20,000$ *cells. Fig. 1 illustrates the similarity between the reference solution and the numerical solution, showing the* η *and* vh *after* $t = 0.1s$ *from the start of the simulation. The comparisons are made using a reference solution obtained by the CNS4 scheme. Accordingly, this allows for an assessment of accuracy, it does not enable a comparison of the presented method's ability with other methods.*

Now, the accuracy analysis results are presented in table 2, demonstrating fourth-order accuracy for all norms and confirming that the scheme's accuracy aligns with the anticipated accuracy. The specific discharge yields comparable outcomes.

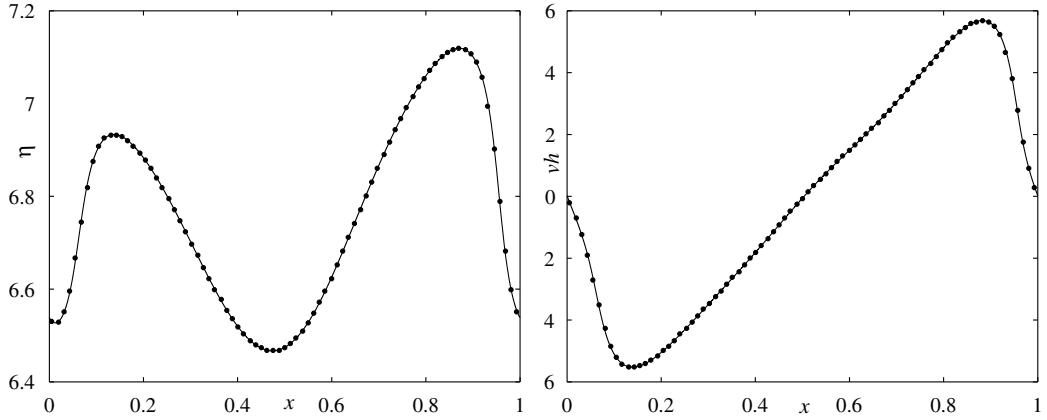

Figure 1: Example 3.2 (unsteady flow over a sinusoidal bump) at the final time $t = 0.1s$. The solid line is "exact solution" and • is "numerical solution".

Table 2: Errors and orders of convergence for Example 3.2 (the free-surface elevation) at $t = 0.1s$

N	L_1 error	L_1 order	L_∞ error	L_∞ order
40	6.07(-4)	—	1.00(-3)	—
80	3.68(-5)	4.04	7.79(-5)	3.68
160	1.84(-6)	4.32	6.24(-6)	3.64
320	1.28(-7)	3.84	5.14(-7)	3.60
640	8.47(-9)	3.92	3.42(-8)	3.91

Example 3.3. *The aim of this example, suggested by authors of [24], is to validate the fulfilment of the C-property by an uneven bottom. Two distinct bottom configurations can be selected as*

$$z(x) = 5\exp\Big(-\frac{2}{5}(x-5)^2\Big)m,$$

which represents a smooth profile, and

$$z(x) = \begin{cases} 4m & x \in [4,8]m, \\ 0 & o.\ w., \end{cases}$$

which is a discontinuous profile. Both cases consider $0 \leq x \leq 10m$. *The initial conditions are characterized by a constant water surface elevation of* $\eta = 10m$ *and zero flow rate. Preserving this initial state of motionlessness is of utmost importance. To assess the scheme's capability to preserve this situation, a demonstration is conducted up to* $t = 0.5s$, *utilizing a mesh comprising* $N = 200$. *The outcomes are summarized in table 3. The dissimilarities between the numerical solution and the reference solution in terms of water depth and flow rate per unit width can be attributed to round-off errors. The obtained results validate the fulfilment of the precise C-property.*

Table 3: C-*property* analysis of h and vh for Example 3.3

	h		vh	
test case	L_1 error	L_∞ error	L_1 error	L_∞ error
smooth	2.89(-13)	2.24(-13)	1.16(-13)	1.76(-13)
non-smooth	3.67(-14)	2.87(-14)	2.03(-14)	2.13(-14)

Example 3.4. *The objective of this example is to verify the treatment of the source component during the demonstration of steady discontinuous flows across an elevation change, as described in [21]. This serves as a standard example for studying transcritical flows. The spatial region comprises a channel with a length of* $25m$, *divided into* 250 *discrete cells. The channel's bottom elevation is considered as follows:*

$$z(x) = \begin{cases} 0.2 - 0.05(x-10)^2 m & x \in [8,12]m, \\ 0 & o.\ w., \end{cases}$$

At $x = 8$ *meters and* $x = 12$ *meters, this equation displays a discontinuous first derivative. In this particular situation, the flow exhibits a transcritical behaviour, characterized by the presence of a constant shock wave formed over the raised surface. The rate of flow per unit area entering the system from the upstream direction is* 0.18 *square meters per second, and the elevation of the water surface on the downstream side is set to* 0.33 *meters. At the beginning of the scenario, the elevation of the free surface is* 0.33 *meters, and there is no flow initially. Fig. 2 exhibits the agreement between the numerical and analytical solutions. The test produces pleasing outcomes concerning the accurate depiction of shock waves and the ability to accurately determine the water levels both upstream and downstream. The position of the discontinuity is precisely represented, with only a small subset of numerical flow discharge values deviating slightly from the analytical solution. However, these discrepancies are mainly observed at the location of the shock wave. Moreover, the satisfaction level of the comparison with analogous numerical findings in the existing literature [21] for the identical experimental scenario is considered acceptable.*

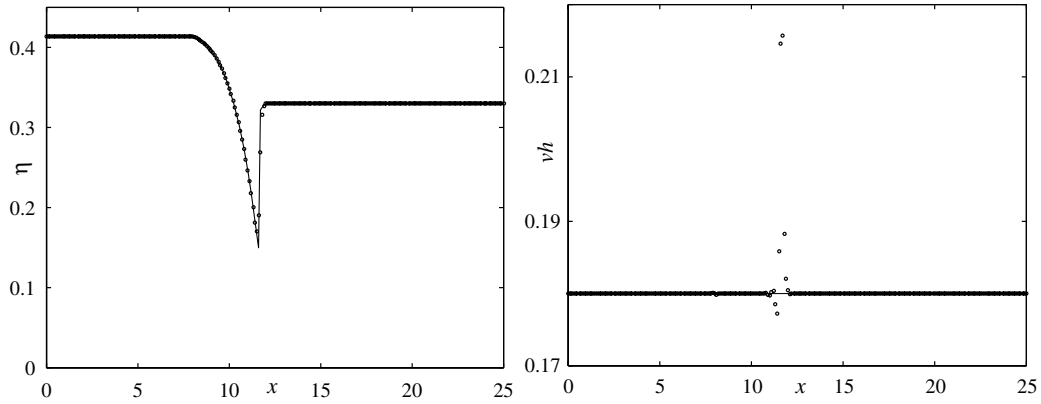

Figure 2: Example 3.4 (parabolic bump-transcritical flow test case). The solid line is "exact solution" and • is "numerical solution".

Now, we aim to validate the fulfilment of the C-property. The initial conditions are characterized by a constant water surface elevation of $\eta = 10m$ *and zero flow rate. To assess the scheme's capability to preserve this situation, a demonstration is conducted up to* $t = 0.5s$, *utilizing a mesh comprising* $N = 250$. *The outcomes are summarized in table 4. The dissimilarities between the numerical solution and the reference solution in terms of water depth and flow rate per unit width can be attributed to round-off errors. The obtained results validate the fulfilment of the precise C-property.*

Table 4: C-*property* analysis of h and vh for Example 3.4

	h		vh	
test case	L_1 error	L_∞ error	L_1 error	L_∞ error
non-smooth	2.19(-12)	4.03(-13)	3.46(-12)	6.81(-14)

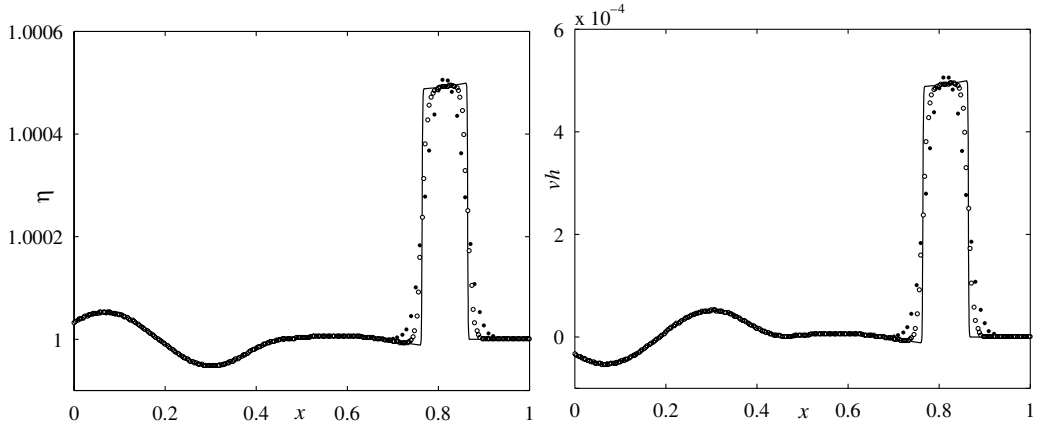

Figure 3: Example 3.5 (pulse over a bump) at the final time $t = 0.7s$. The solid line is "reference solution", • is "numerical solution with 100 cells" and ∘ is "numerical solution with 250 cells".

Example 3.5. *This particular example, suggested by LeVeque [12], is considered to evaluate the scheme's ability to handle the computation of a flow that is not steady occurs over a flat bottom profile. The simulation entails modelling the convective behaviour of a pulse that has an initial size of* 0.1 *meters in length and a height of* 10^{-3} *meters. The pulse moves within a domain that is* 1 *meter in length. Initially, the domain has a calm flow with a depth of* 1 *meter. The simulation duration is* $0.7s$*. The bottom configuration is defined as follows:*

$$z(x) = \begin{cases} 0.25\Big(\cos(10\pi(x-1/2))+1\Big)m & |x-1/2| < 0.1m, \\ 0 & otherwise. \end{cases}$$

The initial disturbance consists of two waves. The wave propagating to the left remains unaffected as it exits the domain, while the wave, as it moves towards the right, interacts with the raised surface or bump. The numerical simulations generated by $N = 100$ *and* $N = 250$ *points are compared with a reference solution generated employing* $N = 5000$ *points. To enable a straightforward comparison with the findings presented by LeVeque [12], the value of gravity has been adjusted to* $1m/s^2$*. The scheme demonstrates overall good performance, notably in areas where the bottom elevation is non-zero, there is a lack of disturbances or variations. This suggests that there is a beneficial equilibrium between the source term and flux gradient when dealing with dynamic or time-varying problems (refer to Fig. 3).*

Example 3.6. *The purpose of this example, as proposed in [23], is to evaluate the model's capability to model the dynamic flow variations occurring over non-uniform bottom profiles. The following equation represents the vertical position of the bed:*

$$z(x) = \begin{cases} 8m & |x-750| \le 187.5m, \\ 0 & otherwise, \end{cases}$$

where $x \in [0, 1500]m$*. The initial functions are considered by:*

$$vh(x,0) = 0, \qquad and \qquad \eta(x) = \begin{cases} 20m & x \le 750m, \\ 15m & o.w.. \end{cases}$$

The simulation duration is $t = 60s$*. The numerical solution is obtained using* $N = 500$ *points and compared with a reference simulation obtained employing* $N = 10000$ *points. The results, shown in Fig. 4, indicate that this particular test case demonstrates the scheme's strong performance. The solution effectively captures the non-smooth regions present in the leading edge of the wave and the lower levels or surfaces. The behaviour of the solution is stable and does not show any oscillations, indicating a consistent match with the reference solution.*

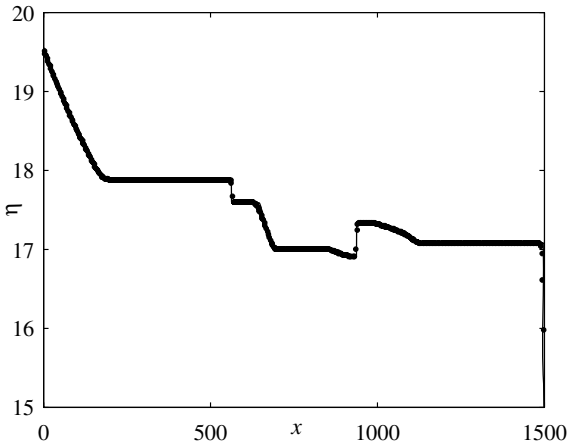

Figure 4: Example 3.6 (dam-break over a rectangular bump) at the final time $t = 60s$. The solid line is "reference solution" and • is "numerical solution".

4. Conclusions

This study presents a new approach that falls within the category of central non-staggered methods. The proposed method achieves fourth-order accuracy in both spatial and temporal domains, rendering it well-suited for numerical integration of the SWE, particularly when dealing with a source component related to bottom slope. The main focus of the study is on a method for handling the source term related to the geometry, which ensures precise preservation of the C-*property* for calm flows across irregular bottom configurations. Furthermore, this approach maintains the fourth-order accuracy in both spatial and temporal domains of the original homogeneous central non-staggered schemes. In order to accomplish this, two accurately balanced central reconstructions are utilized: one of the central reconstructions is employed to calculate the flux derivative at specific points, while the other is used for the spatial integration of the source term. Multiple test problems are employed to assess various aspects, including the accuracy in both space and time, the preservation of the precise fulfilment of the C-*property*, the absence of oscillations, and the capability to effectively resolve shocks.

Acknowledgements

The author is very thankful to the reviewers for carefully reading the paper, their comments and suggestions have improved the quality of the paper.

References

[1] R. Abedian, *A finite difference Hermite RBF-WENO scheme for hyperbolic conservation laws*, Internat. J. Numer. Methods Fluids, 94 (2022), pp. 583–607.

[2] ——, *A modified high-order symmetrical WENO scheme for hyperbolic conservation laws*, Int. J. Nonlinear Sci. Numer. Simul., 24 (2023), pp. 1521–1538.

[3] R. Abedian and M. Dehghan, *The formulation of finite difference RBFWENO schemes for hyperbolic conservation laws: an alternative technique*, Adv. Appl. Math. Mech., 15 (2023), pp. 1023–1055.

[4] A. Bermudez and M. E. Vazquez, *Upwind methods for hyperbolic conservation laws with source terms*, Comput. & Fluids, 23 (1994), pp. 1049–1071.

[5] V. Caleffi, A. Valiani, and A. Bernini, *Fourth-order balanced source term treatment in central WENO schemes for shallow water equations*, J. Comput. Phys., 218 (2006), pp. 228–245.

[6] P. Garcia-Navarro and M. E. Vázquez-Cendón, *On numerical treatment of the source terms in the shallow water equations*, Comput. & Fluids, 29 (2000), pp. 951–979.

[7] A. Harten, B. Engquist, S. Osher, and S. R. Chakravarthy, *Uniformly high-order accurate essentially nonoscillatory schemes. III*, J. Comput. Phys., 71 (1987), pp. 231–303.

[8] A. Harten and S. Osher, *Uniformly high-order accurate nonoscillatory schemes. I*, SIAM J. Numer. Anal., 24 (1987), pp. 279–309.

[9] G.-S. Jiang, D. Levy, C.-T. Lin, S. Osher, and E. Tadmor, *High-resolution nonoscillatory central schemes with nonstaggered grids for hyperbolic conservation laws*, SIAM J. Numer. Anal., 35 (1998), pp. 2147–2168.

[10] G.-S. Jiang and C.-W. Shu, *Efficient implementation of weighted ENO schemes*, J. Comput. Phys., 126 (1996), pp. 202–228.

[11] A. Kurganov and E. Tadmor, *New high-resolution central schemes for nonlinear conservation laws and convection-diffusion equations*, J. Comput. Phys., 160 (2000), pp. 241–282.

[12] R. J. LeVeque, *Balancing source terms and flux gradients in high-resolution Godunov methods: the quasi-steady wave-propagation algorithm*, J. Comput. Phys., 146 (1998), pp. 346–365.

[13] X.-D. Liu and S. Osher, *Nonoscillatory high order accurate self-similar maximum principle satisfying shock capturing schemes. I*, SIAM J. Numer. Anal., 33 (1996), pp. 760–779.

[14] X.-D. Liu, S. Osher, and T. Chan, *Weighted essentially non-oscillatory schemes*, J. Comput. Phys., 115 (1994), pp. 200–212.

[15] X.-D. Liu and E. Tadmor, *Third order nonoscillatory central scheme for hyperbolic conservation laws*, Numer. Math., 79 (1998), pp. 397–425.

[16] C. G. Mingham and D. M. Causon, *High-resolution finite-volume method for shallow water flows*, J. Hydraul. Res., 124 (1998), pp. 605–614.

[17] H. Nessyahu and E. Tadmor, *Non-oscillatory central differencing for hyperbolic conservation laws*, J. Comput. Phys., 87 (1990), pp. 408–463.

[18] A. A. I. Peer, A. Gopaul, M. Z. Dauhoo, and M. Bhuruth, *A new fourth-order non-oscillatory central scheme for hyperbolic conservation laws*, Appl. Numer. Math., 58 (2008), pp. 674–688.

[19] S. Rathan, N. R. Gande, and A. A. Bhise, *Simple smoothness indicator WENO-Z scheme for hyperbolic conservation laws*, Appl. Numer. Math., 157 (2020), pp. 255–275.

[20] S. Rathan and G. Naga Raju, *A modified fifth-order WENO scheme for hyperbolic conservation laws*, Comput. Math. Appl., 75 (2018), pp. 1531–1549.

[21] A. V. Valerio Caleffi and A. Zanni, *Finite volume method for simulating extreme flood events in natural channels*, J. Hydraul. Res., 41 (2003), pp. 167–177.

[22] M. E. Vázquez-Cendón, *Improved treatment of source terms in upwind schemes for the shallow water equations in channels with irregular geometry*, J. Comput. Phys., 148 (1999), pp. 497–526.

[23] S. Vukovic and L. Sopta, *ENO and WENO schemes with the exact conservation property for one-dimensional shallow water equations*, J. Comput. Phys., 179 (2002), pp. 593–621.

[24] Y. Xing and C.-W. Shu, *High order finite difference WENO schemes with the exact conservation property for the shallow water equations*, J. Comput. Phys., 208 (2005), pp. 206–227.

[25] N. K. Yamaleev and M. H. Carpenter, *A systematic methodology for constructing high-order energy stable WENO schemes*, J. Comput. Phys., 228 (2009), pp. 4248–4272.

[26] M. Zennaro, *Natural continuous extensions of Runge-Kutta methods*, Math. Comp., 46 (1986), pp. 119–133.

[27] Z. Zhao, Y. Chen, and J. Qiu, *A hybrid Hermite WENO scheme for hyperbolic conservation laws*, J. Comput. Phys., 405 (2020), pp. 109175, 22.

[28] Z. Zhao and J. Qiu, *A Hermite WENO scheme with artificial linear weights for hyperbolic conservation laws*, J. Comput. Phys., 417 (2020), pp. 109583, 23.

[29] J. G. Zhou, D. M. Causon, D. M. Ingram, and C. G. Mingham, *Numerical solutions of the shallow water equations with discontinuous bed topography*, Int. J. Numer. Methods Fluids, 38 (2002), pp. 769–788.

Please cite this article using:

Rooholah Abedian, Non-oscillatory central schemes for the Saint-Venant system, AUT J. Math. Comput., 6(2) (2025) 97-108
https://doi.org/10.22060/AJMC.2024.22987.1212